A Comparative Study to Reveal the Influence of Typhoons on the Transport, Production and Accumulation of O_3 in the Pearl River Delta, China

Kun Qu[1,2], Xuesong Wang[1,2], Yu Yan[1,2], Jin Shen[3], Teng Xiao[1,2], Huabin Dong[1,2], Limin Zeng[1,2], and Yuanhang Zhang[1,2,4,5]

[1]State Key Joint Laboratory of Environmental Simulation and Pollution Control, College of Environmental Sciences and Engineering, Peking University, Beijing 100871, China
[2]International Joint Laboratory for Regional Pollution Control, Ministry of Education, Beijing, 100816, China
[3]State Key Laboratory of Regional Air Quality Monitoring, Guangdong Key Laboratory of Secondary Air Pollution Research, Guangdong Environmental Monitoring Center, Guangzhou 510308, China
[4]Beijing Innovation Center for Engineering Science and Advanced Technology, Peking University, Beijing 100871, China
[5]CAS Center for Excellence in Regional Atmospheric Environment, Chinese Academy of Sciences, Xiamen 361021, China

Correspondence to: Xuesong Wang (xswang@pku.edu.cn) and Yuanhang Zhang (yhzhang@pku.edu.cn)

Abstract. The Pearl River Delta (PRD) region in South China is faced with severe ambient O_3 pollution in autumn and summer, which mostly coincides with the occurrence of typhoons above the Northwest Pacific. With increasingly severe O_3 pollution in the PRD under the influence of typhoons, it is necessary to gain a comprehensive understanding of the impact of typhoons on O_3 transport, production and accumulation for efficient O_3 reduction. In this study, we analysed the general influence of typhoons on O_3 pollution in the PRD via systematic comparisons of meteorological conditions, O_3 processes and sources on O_3 pollution days with and without typhoon occurrence (denoted as the typhoon-induced and no-typhoon scenarios, respectively), and also examined the differences in these influences in autumn and summer. The results show that the approach of typhoons was accompanied by higher wind speeds and strengthened downdrafts in autumn as well as the inflows of more polluted air masses in summer, suggesting favourable O_3 transport conditions in the typhoon-induced scenario in both seasons. However, the effect of typhoons on the production and accumulation of O_3 were distinct. Typhoons led to reduced cloud cover, and thus stronger solar radiation in autumn, which accelerated O_3 production, but the shorter residence time of local air masses was unfavourable for the accumulation of O_3 within the PRD. In contrast, in summer, typhoons increased cloud cover, and weakened solar radiation, thus restraining O_3 formation, but the growing residence time of local air masses favoured O_3 accumulation. The modelling results using the Community Multiscale Air Quality (CMAQ) model for the typical O_3 pollution days suggest increasing contributions from the transport processes as well as sources outside the PRD for O_3 pollution, confirming enhanced O_3 transport under typhoon influence in both seasons. The results of the process analysis in CMAQ suggest that the chemical process contributed more in autumn but less in summer in the PRD. Since O_3 production and accumulation cannot be enhanced at the same time, the proportion of O_3 contributed by emissions within the PRD was likely to decrease in both seasons. The difference in the typhoon influence on O_3 processes in autumn and summer can be attributed to the seasonal variation of the East Asian monsoon. From the "meteorology-process-source" perspective, this study revealed

the complex influence of typhoons on O_3 pollution in the PRD and their seasonal differences. To alleviate O_3 pollution under typhoon influence, emission control is needed on a larger scale, rather than only within the PRD.

1 Introduction

Tropospheric ozone (O_3) serves as a secondary pollutant in ambient air and is detrimental for human health and crop production (Wang et al., 2017; Liu et al., 2018; Mills et al., 2018). Ambient O_3 is produced from its precursors, i.e., nitrogen oxides (NO_x = NO + NO_2) and volatile organic compounds (VOCs), through chemical reactions in the presence of sunlight. Due to the relatively long lifetime of O_3 (~22 days; Stevenson et al., 2006), it can accumulate locally, or be transported to downwind regions. Under unfavourable meteorological conditions, enhanced transport, production and/or accumulation of O_3 can all contribute to the O_3 pollution within a region (National Research Council, 1991).

As the largest city cluster in South China, the Pearl River Delta (PRD) region is faced with frequent ambient O_3 pollution, especially in autumn and summer (Li et al., 2014; Wang et al, 2017; Lu et al, 2018). Along with the continuous increasing of O_3 levels in recent years (Li et al., 2019), O_3 has become the primary contributor to the deterioration of air quality in this region (Feng et al., 2019). The occurrence of O_3 pollution in the PRD is predominantly related to the influence of typhoons (or tropical cyclones) above the Northwest Pacific (Gao et al., 2018; Deng et al., 2019; Lin et al., 2019). According to Gao et al. (2018), seven out of the nine most severe O_3 episodes (regional-mean maximum 8-h average O_3 concentrations > 240 $\mu g/m^3$) during 2014–2016 coincided with the approach of typhoons. The changes in the track and intensity of typhoons may contribute to the growing trend of O_3 levels recently and in future (Lam, 2018; Lam et al., 2018). Therefore, a comprehensive understanding of the influence of typhoons on the transport, production and accumulation of O_3 has important implications for efficient and strategic O_3 reduction in the PRD.

Analyses of typhoon-related O_3 episodes in the PRD have been extensively reported in previous publications. The effect of typhoons on O_3 pollution is closely linked to meteorological conditions that are conducive to the transport, production and/or accumulation of O_3. Stagnation caused by typhoons, characterised by low wind speeds, has been reported during many episodes, and it promotes the accumulation of locally formed O_3 within the PRD (Wang et al., 1998; So and Wang, 2003; Wang and Kwok, 2003; Huang et al., 2005; Lam et al., 2005; Jiang et al., 2008; Zhang et al., 2014; Chow et al., 2019). Strong north or west winds were observed or simulated during several episodes, suggesting the potentially strengthened transport of pollutants under typhoon influence (Wang et al., 2001; Yang et al., 2012; Wang et al., 2015; Wei et al., 2016). Downdrafts on the outskirts of typhoons may promote downward O_3 transport and contribute to near-ground O_3 pollution as well (Lam, 2018), but its appearance in the PRD has only been examined in a few studies. Cloudless conditions and strong solar radiation enhance O_3 production, which is another important cause of O_3 pollution (Wang et al., 1998; Wang and Kwok, 2003; Li et al., 2018; Yue et al., 2018; Chow et al., 2019). In a more direct way, several studies have utilised

chemical transport models, along with the Process Analysis (PA) tool and source apportionment (SA) methods, to quantify and compare the contributions of various O_3 processes (e.g., transport and the chemical process) and sources (e.g., local emissions, outside emissions and background) during these episodes. Based on reports by Huang et al. (2005), Lam et al. (2005), Jiang et al. (2008), Wang et al. (2010), Li (2013), Wang et al. (2015), Wei et al. (2016) and Chen et al. (2018), horizontal/vertical transport and chemical production may both be the main contributing process for typhoon-induced O_3 pollution in different parts of the PRD. The SA results revealed that emissions within the PRD contributed 40–80% of O_3 during typhoon-related O_3 episodes (Li et al., 2012; Li, 2013; Chen et al., 2015), suggesting the potentially important role of O_3 accumulation for O_3 pollution here. However, despite massive episode-based studies, several important questions still remain: Are O_3 transport, production and accumulation within the PRD all enhanced at the same time by typhoons? Do both O_3 pollution seasons (autumn and summer) experience similar impact of typhoons on O_3 pollution? More thorough investigations are needed to answer these questions.

In this study, we present systematic comparisons between O_3 pollution in the typhoon-induced and no-typhoon scenarios (definitions given in Sect. 2.2) to elucidate the influence of typhoons on O_3 transport, production and accumulation in the PRD and to reveal their seasonal differences. October and July in 2014–2018 were selected as the representative months for autumn and summer, respectively. Multiple datasets, including the ERA-Interim re-analysis, the routine monitoring datasets, trajectories calculated by the Hysplit model and the modelling results of typical O_3 pollution days using the Community Multiscale Air Quality (CMAQ) model, were used in the comparisons. A detailed introduction of these datasets is presented in Sect. 2. The comparisons were conducted from the perspectives of meteorological conditions (Sect. 3), O_3 processes and sources (Sect. 4), and the conclusions about the influence of typhoons on the causes of ambient O_3 pollution in the PRD in the two seasons are illustrated in Sect. 5.

2 Methods

2.1 Datasets

The detailed information for the datasets utilised in the comparison of meteorological conditions is presented below:

- **Re-analysis datasets**: We mainly used the ERA-Interim re-analysis product in the comparisons due to its more available parameters than other re-analysis datasets and high spatial coverage (available at https://www.ecmwf.int/en/forecasts/datasets/reanalysis-datasets/era-interim, last accessed: March 2020; Dee et al., 2011; Berrisford et al., 2011). Specifically, meteorological parameters used in the comparisons include the following three categories: (1) near-surface parameters from the analyses data, including air temperature (at a height of 2 m), relative humidity (RH, at 1000 hPa), horizontal wind speeds (at a height of 10 m; zonal and meridional wind speeds were also involved in the comparisons), and low (for the height at which pressure/surface pressure > 0.8), medium (for the height at which 0.45 < pressure/surface pressure < 0.8), high (for the height at which pressure/surface pressure <

0.45) and total cloud covers; (2) near-surface parameters from the forecast data, including plenary boundary layer (PBL) height and net surface solar radiation; and (3) upper air parameters at multiple heights, including horizontal and vertical wind speeds, cloud water content and O_3 mixing ratio. The focus of this study is O_3 pollution during the daytime, and therefore, only the parameters at 14:00 local time (LT) were selected for the analyses (except for net surface solar radiation, which was averaged within 8:00–17:00 LT).

- **Surface meteorological routine monitoring datasets**: The routine monitoring meteorological data collected at 29 national meteorological sites within the PRD (locations shown in Fig. S1a) were also used to explore the meteorological features under the impact of typhoons. The parameters include air temperature, RH, and wind speed and direction (also transformed to zonal and meridional wind speeds in the comparisons) at 14:00 LT.
- **Typhoon information**: The times, locations and intensities of typhoons were provided by the Chinese Meteorological Administration Best Track Dataset of tropical cyclones (Ying et al., 2014). The tracks of all typhoons that potentially contributed to O_3 pollution in the PRD during the study period (October and July in 2014–2018) are shown in Fig. S2 and S3.
- **O_3 concentrations**: Hourly O_3 concentration data, which were originally released by the China National Environmental Monitoring Centre, were downloaded from http://beijingair.sinaapp.com (last accessed: Dec. 2018). Based on the hourly data, we calculated the maximum 1-hr concentrations (MDA1) and maximum 8-hr average concentrations (MDA8) of O_3 in nine municipalities in the PRD (including Guangzhou, Shenzhen, Zhuhai, Foshan, Jiangmen, Zhaoqing, Huizhou, Dongguan and Zhongshan) to identify O_3 pollution days that served as samples in the comparisons.

2.2 Definition and classification of O_3 pollution days

In this study, O_3 pollution days were defined as the days when the MDA1 exceeds 200 $\mu g/m^3$ or the MDA8 exceeds 160 $\mu g/m^3$ for O_3 (both are the Grade-II thresholds of the Chinese National Ambient Air Quality Standard (NAAQS), GB 3095-2012) in any of the nine municipalities in the PRD. According to these criteria, there were 78 and 55 O_3 pollution days (given in Table S1 and S2) during October and July in 2014–2018, respectively. The information about these O_3 pollution days in the two representative months is listed in Table 1 (overall) and S3 (monthly), including the numbers of days, their proportions in the month, and the corresponding mean O_3 concentrations (MDA8 and MDA1, highest values among nine municipalities in the PRD). Although there were more O_3 pollution days in October than in July, O_3 pollution under typhoon influence occurred on ~30% days of both months. Typhoons tend to result in more severe O_3 pollution in the PRD, as indicated by generally higher O_3 MDA1 and MDA8 values with the influence of typhoons than these without typhoons.

The differing locations of typhoons can result in the diverse effect of typhoons on O_3 pollution (Chow et al., 2018). To determine the general influence of typhoons on O_3 pollution in the PRD, it was necessary to further select O_3 pollution days coinciding with typhoons with similar directions and distances to the PRD. As is shown in Fig. 1, all O_3 pollution days in October and most O_3 pollution days in July under typhoon influence were associated with typhoons to the east of the PRD,

which were more likely to cause O_3 pollution (Chow et al., 2018). In order to minimize the disturbance of typhoon directions in the comparisons, we removed the remaining five O_3 pollution days in July with typhoons located to the due north or southwest of the PRD from the analyses. After this, based on the distances between typhoon centres and the PRD (at 14:00 LT), we classified the pollution days with typhoons in each season into three categories: close typhoon (lowest 20% of distances), typhoon (20–80% intervals of distances), and far typhoon (longest 20% of distances)-induced days. The typhoon-induced days represent O_3 pollution days with general typhoon influence, and they were compared with those without the appearance of typhoons (hereafter denoted as the no-typhoon days). It should be noted that the distances between typhoon centres and the PRD on the typhoon-induced days were overall larger in autumn (1400–2800 km, at 14:00 LT) than in summer (700–2000 km, at 14:00 LT), which may be the consequence of the different characteristics of typhoon paths in the two seasons: most typhoons in autumn travel northwest initially and then turn northward in the areas east of the Philippines (Fig. S2), whereas they are more likely to end up landing in Southeast China in summer (Fig. S3). Since the influence of typhoons on O_3 pollution may be different when typhoons come close enough to the PRD (Lam et al., 2005; Li, 2013), the close typhoon-induced days were considered to be a special scenario in the comparisons of meteorological conditions (Sect. 3.5). Owing to the less apparent effect of typhoons over the PRD, we did not include the far typhoon-induced days in the discussions.

Table 1. The numbers and proportions of O_3 pollution days, and O_3 concentrations for various scenarios.

Parameter	October, 2014–2018	July, 2014–2018
Number (proportion) of O_3 pollution days	78 (50.3%)	55 (35.5%)
With typhoons	49 (31.6%)	45 (29.0%)
Typhoon-induced days	30 (19.4%)	24 (15.5%)
Close typhoon-induced days	10 (6.5%)	8 (5.2%)
Without typhoons (no-typhoon days)	29 (18.7%)	10 (6.5%)
Mean PRD-max O_3 MDA8 ($\mu g/m^3$)		
With typhoons	195.0	205.3
Typhoon-induced days	199.5	205.4
Close typhoon-induced days	184.6	225.7
Without typhoons (no-typhoon days)	189.8	187.8
Mean PRD-max O_3 MDA1 ($\mu g/m^3$)		
With typhoons	230.4	259.8
Typhoon-induced days	235.2	260.0
Close typhoon-induced days	219.2	277.1
Without typhoons (no-typhoon days)	231.5	246.5

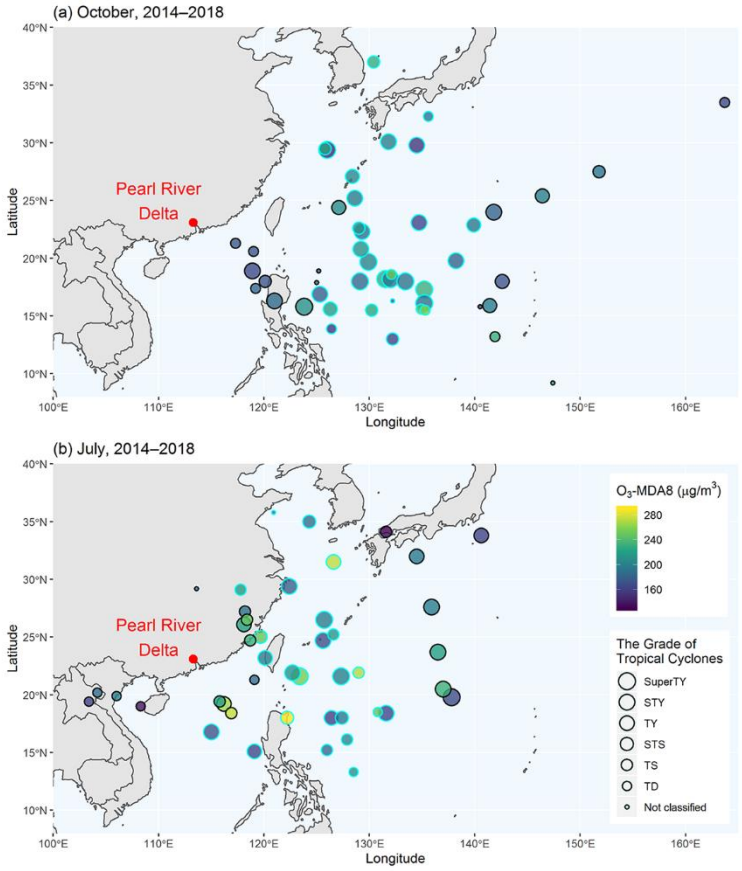

Figure 1. The location and intensity of typhoons at 14:00 LT on all O_3 pollution days with typhoons, and the corresponding O_3 MDA8 concentrations (maximum values in the nine municipalities of the PRD) on the same days during (a) October and (b) July in 2014–2018. The points with cyan borders indicate the "typhoon-induced" O_3 pollution days used in the comparisons. The grades of tropical cyclones (Chinese National Standard, GB/T 19201-2006) are as follows: SuperTY - super typhoon; STY - severe typhoon; TY - typhoon; STS - severe tropical storm; TS - tropical storm; TD - tropical depression; others are grouped as "not classified".

2.3 Calculation of the trajectories and air parcel residence time

To explore the potential effect of cross-regional transport on O_3 pollution in the PRD, we applied the Hysplit model (Stein et al., 2015) with the Global Data Assimilation System (GDAS) datasets as inputs to calculate 72-h backward trajectories reaching the PRD at 14:00 LT for all O_3 pollution days. The Modiesha site (23.1 °N, 113.3 °E; Fig. S1b), which is located in the central part of the PRD, was the endpoint of backward trajectories. Its height was set to 500 m above the ground to indicate the effect of long-range transport on O_3 pollution within the PBL (Park et al., 2007).

Air parcel residence time (APRT), discussed by Huang et al. (2019), is the average number of hours that air parcels originated from one place stay within a pre-defined domain, and long APRTs can be used to indicate good accumulation conditions for locally sourced pollutants. To calculate APRTs in the PRD, we designed a 21×15 point matrix (resolution: 0.2 °×0.2 °) that

embraces the whole PRD (Fig. S4), and forward trajectories starting from these points were also calculated using the Hysplit model. The height of all points was set as 100 m above the ground to represent the height of all local emissions and to reduce the disturbance of the surface, as well. The start times were set as 2:00, 8:00, 14:00 and 20:00 LT for all O_3 pollution days. Afterwards, the length of time each trajectory remained within the administration borders of the PRD, i.e., APRT, was calculated and attributed to its starting point. APRTs in each point were averaged, and these averaged APRT values in all points were interpolated using the Kriging method to obtain field results for the further comparisons.

2.4 CMAQ modelling: basic setups and modelling methods

We utilised the widely used 3D chemical transport model CMAQ (version 5.0.2) to investigate the effects of typhoons on O_3 processes and sources. October 2015 and July 2016 featured the most severe O_3 pollution under typhoon influence among all representative months in autumn and summer, respectively (Table S3). Therefore, O_3 pollution in these two months were modelled and used in further comparisons. Note that the modelling period in autumn was adjusted to 11 October–10 November 2015 to involve more O_3 pollution days (3–5 November 2015). In detail, there were four typhoon-induced O_3 pollution days (14–16 and 21 October 2015) and four no-typhoon O_3 pollution days (28 October and 3–5 November 2015) in October 2015, whereas there were four and six typhoon-induced and no-typhoon days in July 2016, respectively (typhoon-induced: 7–8 and 30–31 July 2016; and no-typhoon: 22–26 and 29 July 2016). The results of daytime (9:00–17:00 LT) O_3 PA and SA on the above O_3 pollution days were averaged for the typhoon-induced and no-typhoon scenarios in autumn (October 2015) and summer (July 2016) and were used in the comparisons.

The main setups of the CMAQ model are presented as follows. Two-nested modelling domains with the resolutions of 36 and 12 km (denoted as d01 and d02, respectively) were set in this study (Fig. 2). Specifically, d02 covers the whole East and Central China (EC-China), enabling us to evaluate the contribution of emissions in these areas to O_3 pollution in the PRD. There were 19 vertical layers in the CMAQ modelling, with about 10 layers within the PBL (about 0–1 km in heights; Guo et al., 2016). The Weather Research and Forecasting (WRF) model (version 3.2) provided the meteorological fields used as inputs. SMOKE (version 2.5) and MEGAN (version 2.10) were used to process the anthropogenic and biogenic emissions, respectively. The anthropogenic emission inventory used in this study consisted of the following three parts: (1) emissions in the PRD, which were provided by the Guangdong Environmental Monitoring Centre; (2) emissions in other areas of mainland China, which were extracted from the MEIC inventory (He, 2012); and (3) emissions in other countries and regions in Asia, which were extracted from the MIX inventory (Li et al., 2017). The initial and boundary conditions of the d01 modelling were obtained from the same-period results of the MOZART-4 global model (available at https://www.acom.ucar.edu/wrf-chem/mozart.shtml, last accessed: Dec. 2019), and those of the d02 modelling were extracted from the d01 modelling results. The SAPRC07 gas-phase chemistry mechanism (Carter, 2010) and the AERO6 aerosol scheme were set in the modelling. In addition, the simulations of the two months were both started 10 days ahead to minimise the disturbance of the bias of the initial conditions. The modelling performances of CMAQ and WRF were determined to be acceptable based on the

comparisons between the observational and modelling series of meteorological parameters, O_3 MDA8, daily NO_2 concentrations and the mixing ratios of non-methane hydrocarbons (NMHCs) in the PRD (for details, refer to Sect. 1 in the Supplement Information), which ensures the validity of the further analyses.

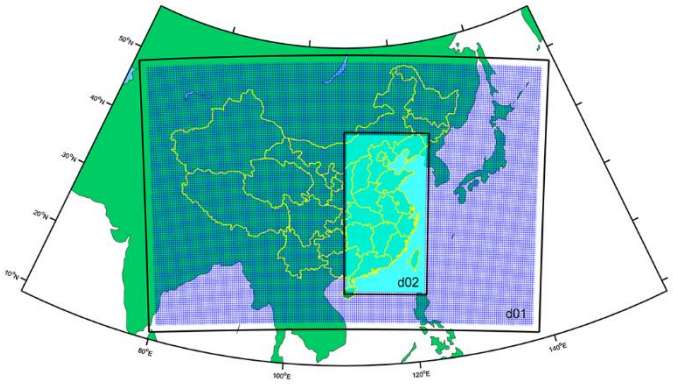

Figure 2. Two-nested modelling domain, noted as d01 and d02. The black boxes indicate the WRF modelling domains, and the nested areas are the CMAQ modelling domains.

The PA tool in CMAQ was implemented to quantify the hourly contributions of O_3 processes (or integrated process rate, IPR), which includes vertical/horizontal transport (convection+diffusion), chemical process (net O_3 production through gas-phase reactions), dry deposition and cloud process. To explore the overall effect of typhoons on O_3 transport and production in the region, the mean PA results within the administration boundaries of the PRD were calculated and compared.

In order to identify the sources of all O_3 in the PRD, we used the classic Brute Force Method (BFM) to identify the contributions of emissions (including anthropogenic and biogenic emissions) in the PRD and other regions in the d02 (mainly EC-China), as well as regions outside the d02 (the boundary conditions of the d02) for O_3 pollution in the PRD (hereafter denoted as the contributions of PRD, EC-China and BCON, or S_{PRD}, $S_{EC\text{-}China}$ and S_{BCON}, respectively). For a pollutant, the contribution of a specific emission, E_i, can be calculated in two ways: (1) the difference between the modelled concentrations of the base case (all emissions involved) and the sensitivity case where E_i is zeroed out (i.e., top-down BFM); (2) the difference between two sensitivity cases where emissions except E_i and all of the emissions are zeroed out, respectively (i.e., bottom-up BFM). Owing to the non-linearity between O_3 and its precursors, biases may occur between the results of two types of BFM methods, leading to the non-additivity of the results (Clappier et al., 2017). Therefore, the average of the top-down and bottom-up BFM results was treated as the quantified contributions of the concerned sources. Four simulation cases were run in this study, including (the modelled O_3 concentration in each case was also marked in brackets):

- the base case (C_{base});
- the PRD-cut case (C_{PRD_cut}), where emissions within the PRD were zeroed out;
- the PRD-only case (C_{PRD_only}), where emissions outside the PRD (within d02) were zeroed out; and

- the zero-emission case (C_0), where all emissions within the d02 were zeroed out.

Afterwards, the S_{PRD}, $S_{EC\text{-}China}$ and S_{BCON} values (in concentrations) in the polluted areas of the PRD (where modelled daytime O_3 concentrations > 160 μg/m^3, the Grade-II O_3 MDA8 thresholds of the Chinese NAAQS) were calculated using the following equations,

$$S_{PRD} = \frac{1}{2}\left[\left(C_{base} - C_{PRD\_cut}\right) + \left(C_{PRD\_only} - C_0\right)\right], \quad \text{(R1)}$$

$$S_{EC-China} = \frac{1}{2}\left[\left(C_{base} - C_{PRD\_only}\right) + \left(C_{PRD\_cut} - C_0\right)\right], \quad \text{(R2)}$$

$$S_{BCON} = C_0. \quad \text{(R3)}$$

The percentage forms of these values were used in the comparisons.

3 Comparison of meteorological conditions

3.1 Overview: comparison of meteorological parameters in the PRD

First, we compared near-ground meteorological parameters in the PRD on the typhoon-induced and no-typhoon O_3 pollution days. Near-surface parameters from routine monitoring datasets and the ERA-Interim re-analysis were used in the comparison. The parameters include air temperature, RH, wind speeds, cloud covers, PBL height and net surface solar radiation. Since there was no rainfall on most O_3 pollution days (indicated by the weather in Guangzhou (Table S4)), precipitation was not considered in the comparisons. For consistency, the parameters of ERA-Interim were extracted at the same time (14:00 LT) and the locations of sites (Fig. S1a) as those in routine monitoring. The Mann-Whitney U test was applied to determine whether the above parameters were significantly different ($p < 0.05$) between typhoon-induced and no-typhoon O_3 pollution days.

As is listed in Table 2, statistically significant differences between the typhoon-induced and no-typhoon scenarios existed for most of the parameters, such as meridional (south-north) wind speed, cloud covers within various height ranges and net surface solar radiation — in both seasons, these parameters were significantly different for the two scenarios. It indicates that the causes of O_3 pollution may vary on typhoon-induced and no-typhoon O_3 pollution days. Note that air temperature, one of the parameters most closely related to O_3 pollution in the PRD (Zhao et al., 2019), was not significantly different in the two scenarios. We also found that the comparison in autumn and summer did not produce the same results: the typhoon-induced days in autumn featured lower RH, stronger winds (especially north wind), reduced cloud cover (low, medium, high and total) and stronger surface solar radiation, whereas in summer, these days had higher RH, weaker south winds, more cloud cover (medium, high and total), weaker surface solar radiation and lower PBL heights. Therefore, the impact of typhoons on O_3 pollution differs in the two seasons, as well. In order to reveal the impact of typhoons on O_3 transport, production, and accumulation in the PRD, more detailed comparisons of the corresponding meteorological indicators are presented in the following sections.

Table 2. The comparisons of meteorological parameters (all at 14:00 LT except for net surface solar radiation, which is the average value for 9:00–17:00 LT) in the PRD for the three scenarios (no-typhoon, typhoon-induced, close typhoon-induced) in two seasons (autumn, summer). RM, routine measurement; ERA, ERA-Interim re-analysis. All of the parameters are presented as "the mean value ± standard deviation". The differences between parameters in the typhoon-induced or close typhoon-induced scenarios and the corresponding typhoon-induced scenarios for the same season are given in parentheses, and "*" indicates $p < 0.05$, or statistically significant differences between these parameters when the Mann-Whitney U test is used.

Parameters	Data Source	Autumn (October, 2014–2018)			Summer (July, 2014–2018)		
		No-typhoon	Typhoon-induced	Close Typhoon-induced	No-typhoon	Typhoon-induced	Close Typhoon-induced
Air Temperature (℃)	RM	29.1 ±2.2	29.3 ±1.8 (+0.2)	29.6 ±1.5 (+0.5, *)	33.7 ±2.0	33.9 ±2.0 (+0.2)	35.0 ±1.5 (+1.3, *)
	ERA	29.2 ±2.1	29.3 ±1.6 (+0.1)	29.6 ±1.5 (+0.4, *)	33.4 ±1.8	33.5 ±1.4 (+0.1)	34.6 ±1.4 (+1.2, *)
RH (%)	RM	52.4 ±10.2	44.8 ±10.4 (-7.6, *)	51.4 ±12.4 (-1.0)	57.0 ±9.3	58.3 ±9.7 (+1.3)	56.9 ±6.4 (-0.1)
	ERA	54.0 ±9.8	48.3 ±11.2 (-5.7, *)	52.2 ±12.4 (-1.8, *)	62.6 ±10.8	66.4 ±9.4 (+3.8, *)	62.5 ±9.4 (+0.1)
Wind Speed (m/s)	RM	2.33 ±1.18	2.58 ±1.23 (+0.25, *)	2.96 ±1.40 (+0.63, *)	2.46 ±1.33	2.30 ±1.20 (-0.16)	2.53 ±1.16 (+0.07)
	ERA	2.39 ±1.30	2.54 ±0.99 (+0.15, *)	3.53 ±1.11 (+1.14, *)	2.41 ±0.99	2.18 ±1.18 (-0.23, *)	2.61 ±1.05 (+0.20)
Zonal (East-West) Wind Speed (m/s)	RM	-0.83 ±1.72	-0.59 ±1.70 (+0.24, *)	-0.13 ±1.74 (+0.70, *)	-0.41 ±2.05	-0.03 ±1.94 (+0.38)	0.73 ±1.98 (+1.14, *)
	ERA	-1.41 ±1.43	-1.07 ±1.04 (+0.34, *)	-0.87 ±0.79 (+0.54, *)	0.22 ±1.73	-0.02 ±1.81 (-0.24)	0.29 ±2.45 (+0.07)
Meridional (South-North) Wind Speed (m/s)	RM	-0.36 ±1.74	-1.49 ±1.66 (-1.13, *)	-2.21 ±1.66 (-1.85, *)	0.79 ±1.69	0.01 ±1.72 (-0.78, *)	-0.69 ±1.68 (-1.48, *)
	ERA	-0.27 ±1.82	-1.97 ±1.16 (-1.70, *)	-3.27 ±1.29 (-3.00, *)	1.61 ±1.09	0.64 ±1.58 (-0.97, *)	-0.68 ±1.19 (-2.29, *)
Low Cloud Cover (%)	ERA	17.2 ±22.7	4.2 ±11.9 (-13.0, *)	15.5 ±23.9 (-1.7, *)	8.7 ±9.4	7.1 ±9.5 (-1.6, *)	5.2 ±5.0 (-3.5, *)
Medium Cloud Cover (%)	ERA	22.2 ±26.5	10.4 ±19.7 (-11.8, *)	9.5 ±14.5 (-12.7, *)	8.7 ±11.1	15.4 ±15.1 (+6.7, *)	21.5 ±15.5 (+12.8, *)
High Cloud Cover (%)	ERA	12.1 ±23.1	7.2 ±16.3 (-4.9, *)	34.6 ±35.6 (+22.5, *)	32.2 ±30.0	44.9 ±29.3 (+12.7, *)	51.0 ±34.2 (+18.8, *)
Total Cloud Cover (%)	ERA	43.5 ±32.3	20.5 ±25.7 (-23.0, *)	51.9 ±33.1 (+8.4, *)	43.7 ±26.7	58.3 ±22.7 (+14.6, *)	67.5 ±21.0 (+23.7, *)
Net Surface Solar Radiation (W/m^2)	ERA	456.9 ±78.4	516.6 ±66.7 (+59.7, *)	516.5 ±62.8 (+59.6, *)	560.3 ±93.1	523.2 ±74.4 (-37.1, *)	541.9 ±54.0 (-18.4, *)
PBL Height (m)	ERA	1471 ±315	1473 ±348 (+2)	1349 ±227 (-122, *)	1268 ±383	1037 ±289 (-231, *)	1196 ±300 (-72, *)

3.2 O_3 transport conditions: comparison of wind speeds, backward trajectories and vertical air motions

The higher wind speeds and/or O_3 levels in the transported air masses are, the more likely O_3 transport plays an increasingly important role in O_3 pollution. In the PRD, O_3 levels are closely linked to the type of air masses influencing the region, which

can be identified based on backward trajectories. According to Zheng et al. (2010), there are generally three types of air masses that are transported into the PRD along different paths and contribute to O_3 pollution here, namely, the continental, coastal and marine air masses (Fig. 3a). The continental and coastal air masses can bring O_3 from EC-China to the PRD, and thus, they are typically recognised as being polluted and contributing to relatively high O_3 levels in the PRD. In contrast, the marine air masses, originated from the South China Sea, are much cleaner. In this section, we studied the influence of typhoons on O_3 transport by comparing wind speeds and 72-h backward trajectories in the typhoon-induced and no-typhoon scenarios.

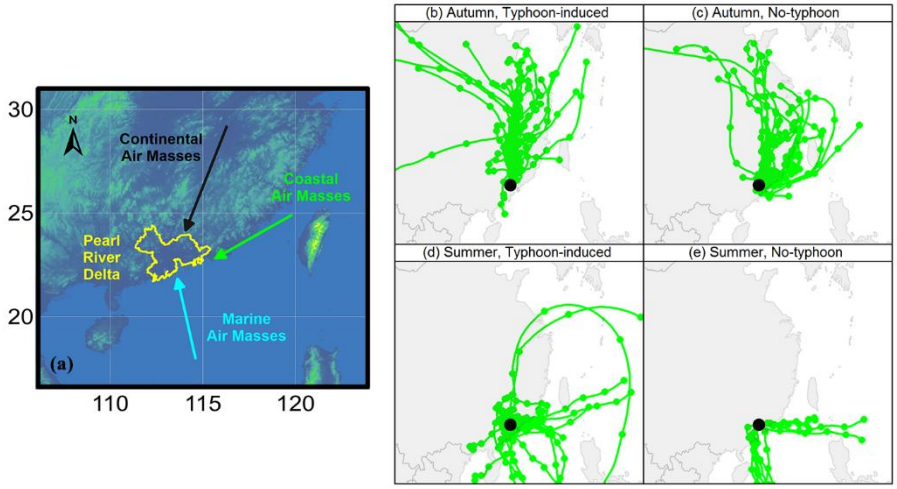

Figure 3. (a) Three O_3 transport paths towards the PRD. (b–e) Backward trajectories at 14:00 LT for each scenario: (b) autumn, typhoon-induced; (c) autumn, no-typhoon; (d) summer, typhoon-induced; and (e) summer, no-typhoon. The black dots indicate the end point of all trajectories, i.e., where the Modiesha site in the central PRD is located.

As is displayed in Fig. 3b–c, we identified the influence of continental air masses on the typhoon-induced O_3 pollution days in autumn, as well as mixed contributions from the continental and coastal air masses on the corresponding no-typhoon days. However, for the former scenario, significantly increased wind speeds (Table 2) ensure more favourable conditions for the transport of O_3. In summer, the three types of air masses may all have affected O_3 pollution in the typhoon-induced scenario, while only the marine air masses influenced the PRD in the no-typhoon scenario (Fig. 3d–e). The increasing influence of much more polluted air masses (continental and coastal air masses) led by typhoon ensured that more O_3 was transported to the PRD, thus typhoons also tended to increase the contribution of transport to O_3 pollution in the PRD in summer. In addition, the influence of different air masses was also accompanied with variations in the prevailing winds in the PRD, that is, north winds and easterlies in the typhoon-induced and no-typhoon scenarios in autumn, respectively, and southerly winds in the no-typhoon scenario in summer (indicated by wind roses in Fig. S5). For the typhoon-induced scenario in summer, the dominate wind direction is hard to determine. These variations in the local wind fields potentially result in the different spatial distribution of O_3 concentrations in various scenarios.

Downdrafts are typically considered to be an important cause of typhoon-induced O_3 pollution (Lam, 2018), but in which scenarios downdrafts influence the PRD remains unclear. Thus, we explored the overall features of vertical air motions from the surface layer to the tropopause in the typhoon-induced and no-typhoon scenarios, and the ERA-Interim reanalysis dataset (including all upper air parameters at multiple heights introduced in Sect. 2.1) was utilised in the comparisons. The contours in Fig. 4 show the cross sections of mean vertical wind speed at 14:00 LT of all O_3 pollution days corresponding to the typhoon-induced and no-typhoon scenarios of two seasons, which were made along the 113.2 °E longitude line, from 26.0 °N to 20.0 °N (Fig. S4). On the typhoon-induced days in autumn, downdrafts occurred over large areas above the PRD, especially above a height of ~700 hPa. Although updrafts can still be found near the sea surface in this scenario, vertical wind speeds tended to be lower compared with those on the no-typhoon days in autumn, which also suggests the enhancement of downdrafts caused by typhoons. In summer, the influence of downdrafts was found over the PRD under 850 hPa on the typhoon-induced O_3 pollution days. However, overall, updrafts prevailed above the land areas and downdrafts prevailed above the sea in both the typhoon-induced and no-typhoon scenarios in summer, which is recognised as the structure of the East Asian summer monsoon cell (Chen et al., 1964; Jin et al., 2013; Ding et al., 2018). For both updrafts and downdrafts, the absolute values of vertical wind speeds in the typhoon-induced scenario in summer were overall higher than those in the corresponding no-typhoon scenario. Therefore, the approach of typhoons did not break the structure of the summer monsoon cell, but rather they further strengthened the vertical motions above both land areas and sea. These analyses suggest that typhoons do not necessarily lead to downdrafts during O_3 pollution periods in the PRD and its adjacent areas; and in summer, vertical air motions affected by typhoons are more complicated than expected owing to the existence of the East Asian summer monsoon.

We also explored the regions where downdrafts and updrafts occurred on a larger scale and their potential connections with O_3 levels. As is shown in Fig. 5, though updrafts appeared in the PRD at 850 hPa on the typhoon-induced days in autumn, downdrafts dominated in the region at 700 and 500 hPa. For the areas to the north of the PRD, the important role of downdrafts was found at all three heights. In contrast to the no-typhoon days in autumn, downdrafts tended to cover much larger areas in this scenario. Moreover, these areas at 850 and 700 hPa generally featured higher O_3 mixing ratios as well as lower RH (Fig. S6) than others, which is a sign of possible direct downward O_3 transport (Roux et al., 2020; Wang et al., 2020). This part of O_3 can notably aggravate near-ground O_3 pollution in the PRD. In contrast, in summer, updrafts dominated the PRD at various heights in both scenarios. Besides the PRD, most of the regions near the coast were characterised by updrafts above the land as well as downdrafts offshore, further indicating the ubiquity of the summer monsoon cell. By comparing the two scenarios in summer, we found that typhoons resulted in more areas being influenced by updrafts. The areas with high O_3 levels did not coincide with the downdraft-affected areas, and therefore, O_3 transported from the upper air may play a less significant role in the typhoon-induced O_3 pollution in summer.

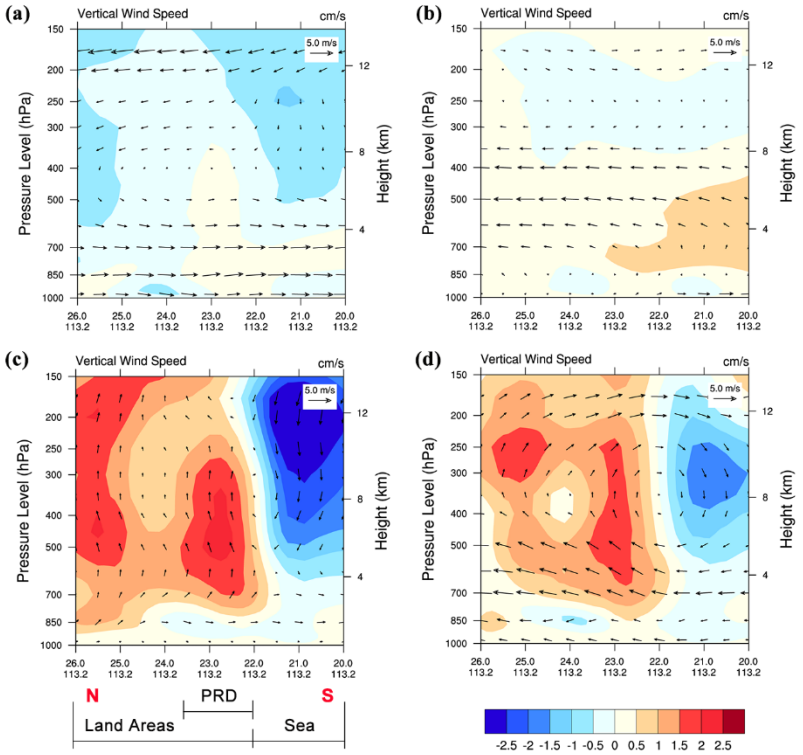

Figure 4. The cross sections of mean vertical wind field at 14:00 LT for each scenario: (a) autumn, typhoon-induced; (b) autumn, no-typhoon; (c) summer, typhoon-induced; and (d) summer, no-typhoon. Cross sections were made along the 113.2 °E longitude line, from 26.0 °N to 20.0 °N (Fig. S4). The vectors indicate meridional wind speed (m/s) and vertical wind speed (cm/s), and the contours indicate vertical wind speed (cm/s). PRD, the Pearl River Delta.

3.3 O_3 production conditions: comparison of clouds

Clouds efficiently reflect solar radiation (Liou, 1976), and therefore, they have a notable impact on the local formation of O_3. Figure 6 displays the cross sections of mean ERA-Interim cloud liquid water contents (CLWC) at 14:00 LT of all O_3 pollution days corresponding to the typhoon-induced and no-typhoon scenarios of two seasons, which were also made along the 113.2 °E longitude line, from 26.0 °N to 20.0 °N (Fig. S4). The comparison of CLWC in the cross sections suggests that typhoons generally resulted in fewer clouds in autumn but more clouds in summer, which agrees well with the comparison of cloud covers in Table 2. The presence of fewer clouds on the typhoon-induced days in autumn can be attributed to two reasons: the influence of dry air masses (indicated by lower RH in Table 2 and Fig. S6) and/or the hindrance of cloud formation by downdrafts. In summer, the strengthened updrafts above the land caused by typhoons favoured cloud formation, which is demonstrated by higher CLWC at the heights of 500–850 hPa and increases in medium and high cloud covers. In areas above the PRD below 850 hPa, downdrafts led to slight decrease of clouds in the typhoon-induced scenario in summer, which is also indicated by reduced low cloud cover. As a consequence of varied cloud covers in each scenario, on average, net surface solar

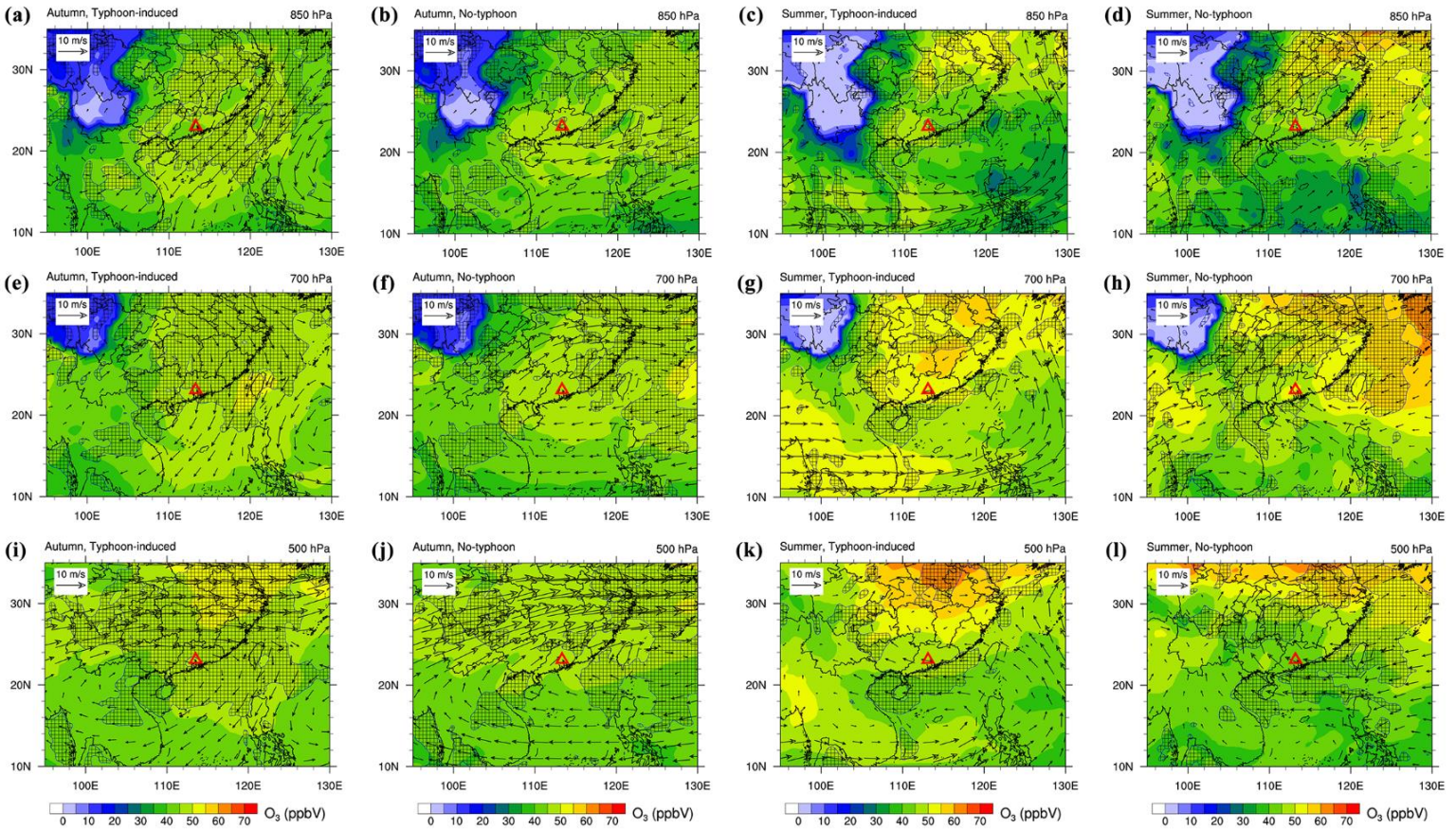

335

336 **Figure 5.** O_3 mixing ratio (ppbV) and wind fields at the height of (a–d) 850 hPa, (e–h) 700 hPa, and (i–l) 500 hPa at 14:00 LT for each scenario: (a, e, i) autumn,
337 typhoon-induced; (b, f, j) autumn, no-typhoon; (c, g, k) summer, typhoon-induced; and (d, h, l) summer, no-typhoon. The red triangle in each plot indicates the
338 PRD. The gridded areas indicate that vertical wind speed is less than 0, or downdrafts occur.

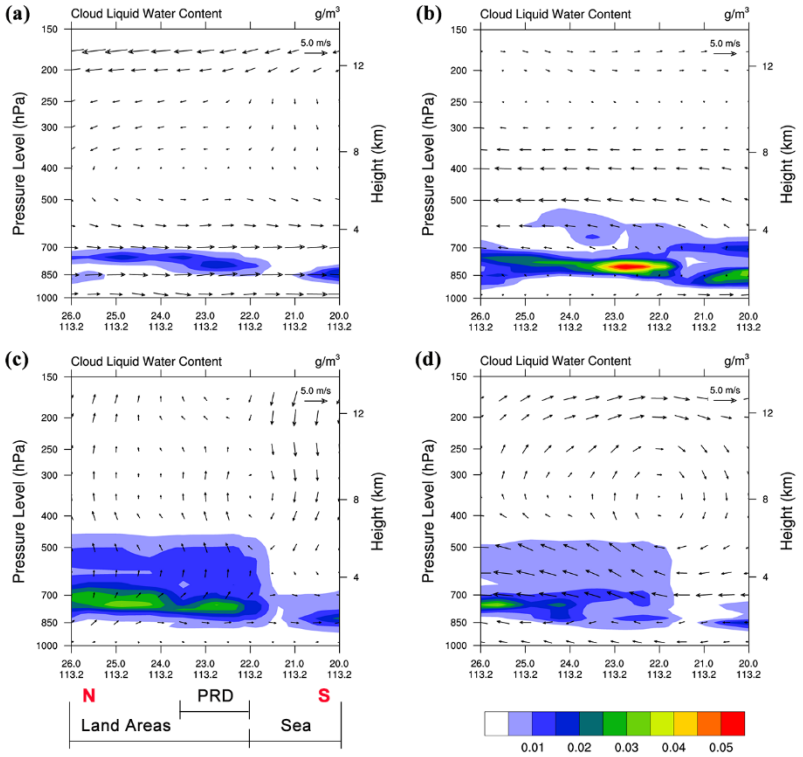

Figure 6. The cross sections of mean cloud liquid water content (g/m^3) and wind vectors at 14:00 LT for each scenario: (a) autumn, typhoon-induced; (b) autumn, no-typhoon; (c) summer, typhoon-induced; and (d) summer, no-typhoon. Cross sections were made along the 113.2 °E longitude line, from 26.0 °N to 20.0 °N (Fig. S4). The vectors indicate meridional wind speed (m/s) and vertical wind speed (cm/s). PRD, the Pearl River Delta.

radiation increased by 13% and decreased by 7% on the typhoon-induced days in autumn and summer, respectively (Table 2), which promoted and hindered O_3 production in the PRD during these two seasons, respectively.

3.4 O_3 accumulation conditions: comparison of APRTs

The longer APRTs are, the more likely that O_3 produced by local emissions accumulates within the targeted region and notably contributes to near-ground O_3 pollution. In order to study the effect of typhoons on O_3 accumulation, we calculated APRTs in the PRD in the typhoon-induced and no-typhoon scenarios (Fig. 7) for the further comparisons. On the typhoon-induced days in autumn, APRTs were typically 5–10 hours (mean = 9.5 hours) — shorter than those on the no-typhoon days in autumn (mean = 13.1 hours). In addition, lower APRT values occurred in the central part of the PRD, where high anthropogenic emissions of pollutants are distributed (Zheng et al., 2009). Despite more active O_3 chemistry discussed in the last section, locally sourced O_3 was less likely to accumulate within the PRD in this scenario, potentially limiting the contribution of local emissions for O_3. The comparison suggests opposite results in the summer scenarios, that is, APRTs on the typhoon-induced days (20–30 hours, mean = 21.0 hours) were overall higher than those on the no-typhoon days (15–25 hours, mean = 16.5 hours). This favoured the accumulation of locally sourced O_3. Based on the comparisons in this and previous section, typhoons

did not provide more favourable conditions for O_3 production and accumulation simultaneously in the PRD in both autumn and summer, thus potentially resulting in reduced contributions in percentage of local emissions to O_3 pollution here. More quantitative evaluations of the contributions from multiple O_3 sources are discussed in Sect. 4.

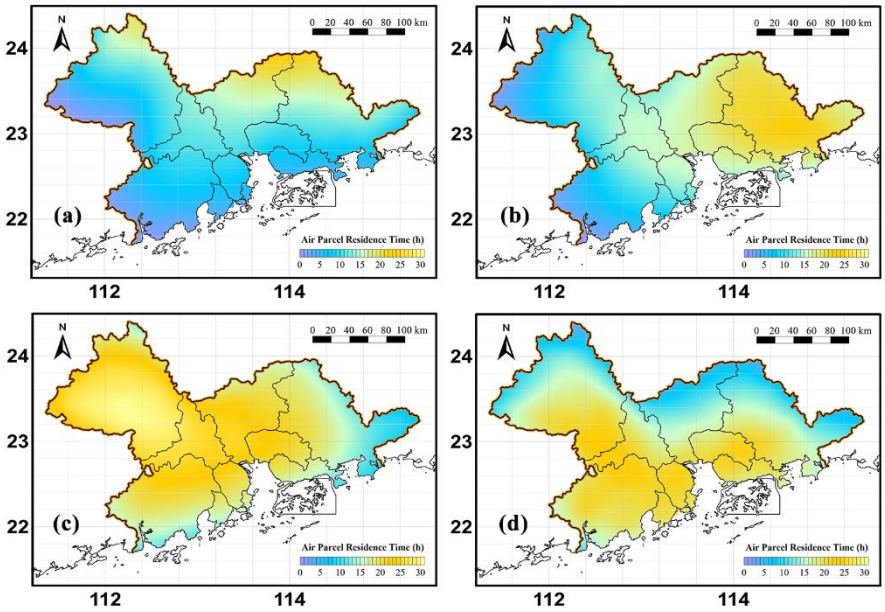

Figure 7. The spatial distributions of APRTs in the PRD for each scenario: (a) autumn, typhoon-induced; (b) autumn, no-typhoon; (c) summer, typhoon-induced; and (d) summer, no-typhoon.

3.5 Meteorological conditions on the close typhoon-induced days

On the close typhoon-induced days in the two seasons, stronger north winds prevailed and total cloud cover was higher than that on the no-typhoon days (Table 2), suggesting better conditions for the transport of O_3 but less favourable conditions for O_3 production. As displayed in Fig. S7, the APRT values were significantly lower on the close typhoon-induced days (mean = 6.6 hours, 12.9 hours in autumn and summer, respectively) than on the no-typhoon days, making it even harder for locally sourced O_3 to accumulate within the PRD. Therefore, close typhoons are concluded to promote the transport of O_3 from the outside and to reduce the contributions of O_3 produced from local emissions in a more notable way. In addition, close typhoons led to stronger downdrafts in autumn and updrafts in summer than other scenarios in the same season (Fig. S8). It should be noted that the structure of the summer monsoon cell near the PRD was destroyed in the close typhoon-induced scenario in summer, indicating the stronger influence of typhoons on regional wind fields. The dominant role of O_3 transport during O_3 pollution days in this special scenario agrees well with the reported episode-based analyses (Lam et al., 2005; Li, 2013).

4 Comparisons of O_3 processes and sources

The comparisons of meteorological conditions served as qualitative evidence to determine the general influence of typhoons on O_3 transport, production and accumulation in autumn and summer. Based on the comparison between the CMAQ modelling results on typical O_3 pollution days in October 2015 and July 2016, more quantitative evidence can be presented. Figure 8 displays modelled mean O_3 MDA8 concentrations and wind fields (at 14:00 LT) on the typhoon-induced and no-typhoon O_3 pollution days of two seasons. Large standard-exceedance (> 160 μg/m^3) areas were distributed in the PRD on most days, and the typhoon-induced days of both seasons generally featured higher O_3 levels. The distinct wind fields for these scenarios, which were consistent with those in the longer timespan (Fig. S5), indeed led to different spatial distributions of O_3. Generally, the most severe O_3 pollution occurred in the downwind areas, such as the central and southern parts of the PRD on the typhoon-induced days in October 2015, the central PRD on the no-typhoon days in October 2015, and the northern and eastern PRD on the no-typhoon days in July 2016. On the typhoon-induced days in July 2016, high levels of O_3 accumulated around the PRE. In this section, we discuss the different contributions of various O_3 processes and sources on these days to better understand the effect of typhoons on O_3 pollution in the PRD.

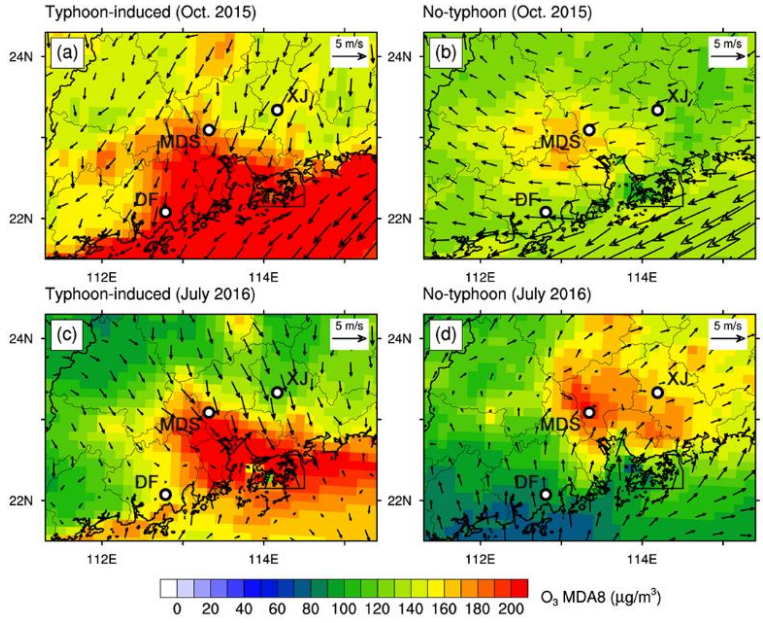

Figure 8. Modelling mean O_3 MDA8 concentrations (μg/m^3) and wind vectors (at 14:00 LT) on the representative O_3 pollution days: (a) the typhoon-induced days in October 2015 (14–16 and 21 October 2015); (b) the no-typhoon days in October 2015 (28 October and 3–5 November 2015); (c) the typhoon-induced days in July 2016 (7–8 and 30–31 July 2016); and (d) the no-typhoon days in July 2016 (22–26 and 29 July 2016). Three representative sites in the PRD are shown as black circles in the plots: XJ, Xijiao; MDS, Modiesha; DF, Duanfen.

4.1 O_3 processes: transport vs chemical process

The PA tool in CMAQ was used to quantify the contributions of transport and chemical process to the O_3 variations on O_3 pollution days in October 2015 and July 2016. As is shown in Fig. 9, the daytime (9:00–17:00 LT) O_3 PA results within the PRD in all scenarios share similar characteristics. Dry deposition dominated O_3 removal near the surface, and it also led to high gradients of O_3 concentrations that promote downward O_3 diffusion. Within the PBL (about 0–1 km in height), O_3 was mainly contributed by horizontal transport and chemical process, and vertical convection led to the drop of O_3 concentrations. However, differences existed between the O_3 PA results in the typhoon-induced and no-typhoon scenarios, indicating the impact of typhoons on the transport and production of O_3. In both months, typhoons led to notably higher contribution of horizontal transport to O_3, especially in the lower and middle part of the PBL. Within the PBL, on average, it increased from -0.9 ppb/h, -0.8 ppb/h to 1.2 ppb/h, 2.0 ppb/h under typhoon influence in autumn and summer, respectively. The comparison of the contribution of chemical process (in absolute rates) suggests that they had opposite effects in the two months — under typhoons, the contribution increased in October 2015 (from 4.0 ppb/h to 4.5 ppb/h within the PBL, or by 11.4%), but it decreased in July 2016 (from 7.1 ppb/h to 5.7 ppb/h within the PBL, or by -20.8%). In other words, typhoons promoted and hindered O_3 production in autumn and summer, respectively. These results agree well with the comparisons of O_3 transport and production conditions in the previous section.

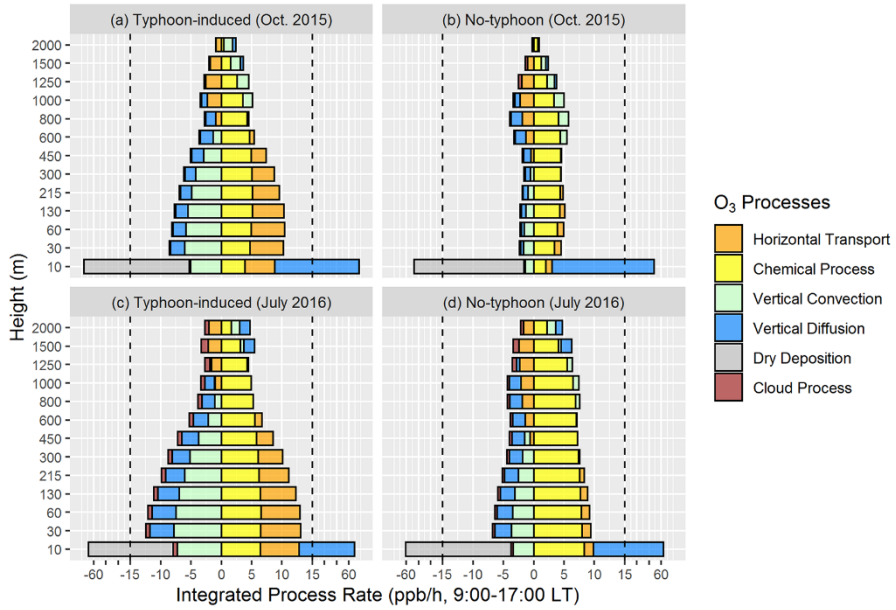

Figure 9. The daytime-mean (9:00–17:00 LT) hourly contributions of O_3 processes within the PRD in vertical layers 1–13 on representative O_3 pollution days: (a) the typhoon-induced days in October 2015 (14–16 and 21 October 2015); (b) the no-typhoon days in October 2015 (28 October and 3–5 November 2015); (c) the typhoon-induced days in July 2016 (7–8 and 30–31 July 2016); and (d) the no-typhoon days in July 2016 (22–26 and 29 July 2016).

4.2 O_3 sources: local sources vs regional sources

The contributions of various sources to O_3 within the PRD are determined by the combined impact of O_3 transport, production and accumulation. The results for mean daytime (9:00–17:00 LT) O_3 SA near the ground (about 0–80 m in height) on typhoon-induced and no-typhoon O_3 pollution days are illustrated in Fig. 10. For polluted regions within the PRD, stronger O_3 production under typhoons did not lead to a higher proportion of local contributions to O_3 pollution in October 2015 — it even decreased from 22% (on the no-typhoon days) to 17% (on the typhoon-induced days). The contributions of EC-China emissions and BCON, in contrast, increased slightly from 37%, 41% to 40%, 43%, respectively. The distinction of the O_3 SA results is more apparent for the summer scenarios, that is, typhoons resulted in growing contributions from O_3 transported from other regions (from 40% to 59%) but decreased local contributions (from 60% to 41%) in July 2016. More favourable O_3 accumulation conditions (indicated by higher APRTs on the representative typhoon-induced O_3 pollution days in summer (Fig. S9)) were far from sufficient to compensate for the effect of weakened O_3 production on the high contributions of local sources.

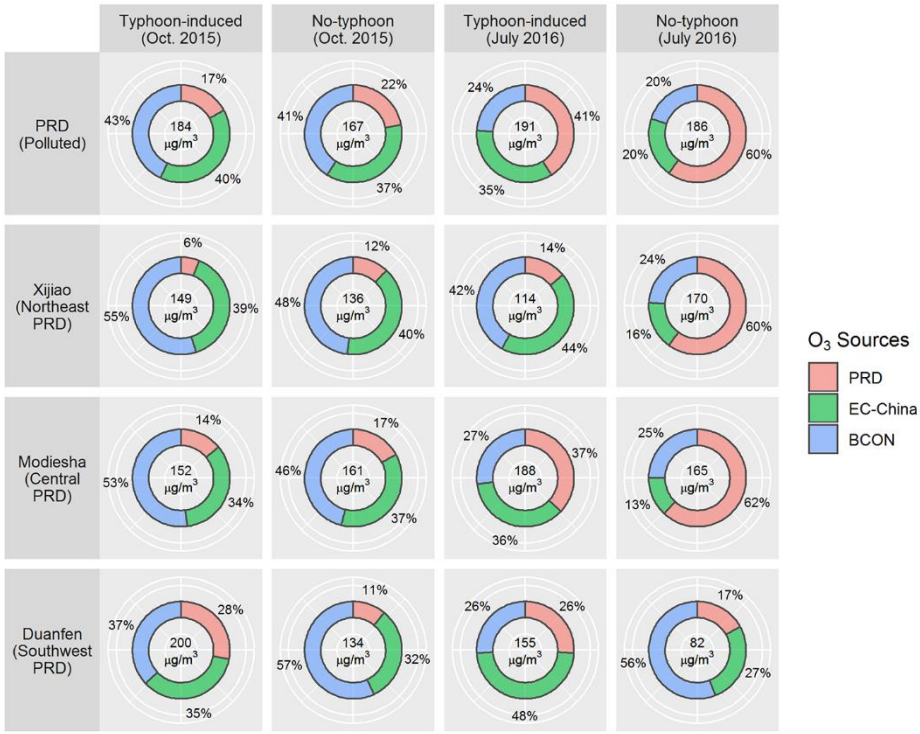

Figure 10. The mean O_3 SA near the ground (about 0–80 m in height) on the represented typhoon-induced and no-typhoon O_3 pollution days in October 2015 and July 2016 (the average results of 9:00–17:00 LT). The locations of the three representative sites (Xijiao, Modiesha and Duanfen) are shown in Fig. 8. PRD, the Pearl River Delta; EC-China, East China and Central China; BCON, the boundary conditions of the d02 modelling.

Furthermore, owing to the variations of wind fields, the comparison results of O_3 SA in different parts of the PRD may differ from the regional ones. For instance, while the comparisons of O_3 SA in the Xijiao and Modiesha site (located in the northeast

and central part of the PRD, respectively) agree well with those in the polluted regions of the PRD, higher contributions of PRD emissions for O_3 can be found in the Duanfen site (located in the southwest part of the PRD) on the typhoon-induced days of two months in comparison to these on the corresponding no-typhoon days (Fig. 10). Since the site was located in the downwind region in the typhoon-induced scenario in October 2015 (Fig. 8a), enhanced O_3 production led by typhoons from the massive emissions of O_3 precursors in the central PRD (Zheng et al., 2009) contributed to higher local contributions for O_3 pollution here (as the distribution of local contributions in percentage to daytime O_3 shown in Fig. S10, the highest local contribution in the PRD occurred in areas near the Duanfen site and almost reached 40% in this scenario, which was even higher than that in the corresponding no-typhoon scenario (33%)). In the no-typhoon scenario in July 2016, the site was located in the upwind regions under the prevailing of southerly winds, limiting the contributions of local emissions for O_3 at the site (Fig. 8d). Thus, higher local contributions can also be found in the typhoon-induced scenario in this month.

5 Discussion and conclusions

The significance of typhoons on O_3 pollution in the PRD calls for thorough evaluations of the different causes of O_3 pollution with the appearance of typhoons in the Northwest Pacific. In this study, we revealed the different impacts of typhoons on O_3 transport, production and accumulation in the PRD (as summarised in Fig. 11) through systematic comparisons of meteorological conditions, the contributions of various O_3 processes and sources in the typhoon-induced and no-typhoon scenarios. We found that typhoons tended to promote O_3 transport towards the PRD, but failed to provide more favourable O_3 production and accumulation conditions simultaneously, which limited the contribution of local emissions to O_3 pollution. Furthermore, there were also differences between the influence of typhoons on O_3 pollution in autumn and summer. More favourable transport conditions occurred in the typhoon-induced scenario in autumn, which was characterised by higher wind speeds and the increased influence of downdrafts. In summer, the mixed types of air masses in the typhoon-induced scenario were likely to bring more O_3 into the PRD than the clean marine air masses in the no-typhoon scenario, also suggesting enhanced O_3 transport under the influence of typhoons. Generally, typhoons led to cloudless conditions, stronger solar radiation, and thus more rapid O_3 production in autumn, but shorter APRTs (5–10 hours) suggest that locally sourced O_3 was hard to accumulate within the PRD. As a result, the contributions in percentage of local emissions to O_3 pollution decreased (slightly by ~5% for the polluted regions of the PRD in October 2015). In contrast, in summer, intensified updrafts associated with typhoons strengthened cloud formation, weakened solar radiation, and thus restrained local O_3 production. Longer APRTs (> 20 hour) under typhoon influence were far from sufficient to maintain high contributions of local emissions for O_3 pollution (which decreased by ~20% for the polluted regions of the PRD in July 2016). However, due to the variations of wind fields under different scenarios, the changes of local and transport contributions for O_3 led by typhoons were different in the southwest part of the PRD, that is, higher contribution from emissions within the PRD and reduced transport contribution occurred in the typhoon-induced scenarios in both seasons. As for the close typhoon-induced scenario, O_3 transport was further

strengthened, but meteorological conditions in the PRD became less favourable for both the production and accumulation of O_3.

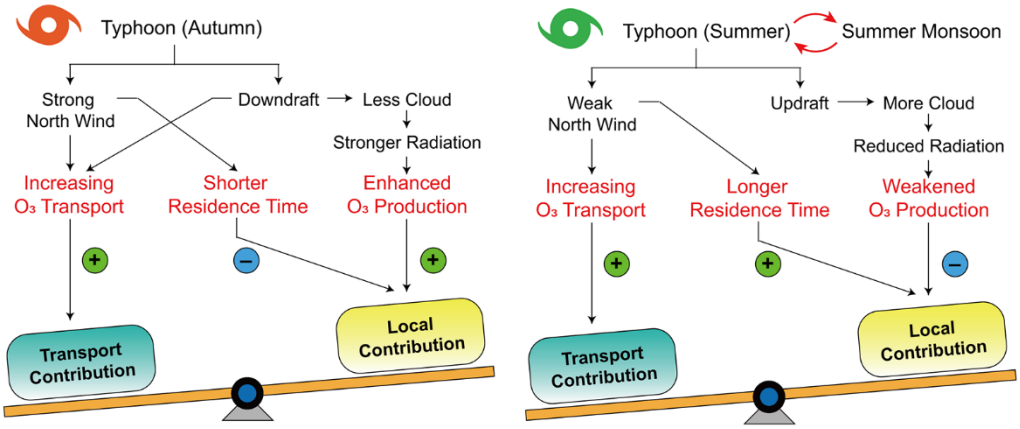

Figure 11. The summary of the causes of O_3 pollution in the PRD under typhoon influence in autumn and summer.

The East Asian monsoon, changing with seasons, has a pronounced impact on local meteorological conditions as well as the characteristics of O_3 pollution in East China (He et al., 2008). The seasonal behaviour of the East Asian monsoon is likely to result in the seasonally varied effect of typhoons on O_3 pollution in the PRD. In October, the summer monsoon has almost finished its retraction and the winter monsoon is beginning (Ding, 1994). Thus, there are not many obstacles to the southward movement of typhoon periphery and the transport of O_3 towards the PRD by the continental and coastal air masses. Large downdraft-influenced areas in Central and South China occur in this scenario, and high O_3 levels and low RH in these areas indicate the potentially important role of directly downward O_3 transport. In July, the summer monsoon reaches its strongest (Ding, 1994). The interaction between typhoon periphery and the summer monsoon results in stagnation and enhanced updrafts above the land areas of the PRD and its surroundings. Only when typhoon is close enough to the PRD is the stagnation terminated and the structure of the summer monsoon cell broken. This also explains why some summertime typhoon-induced O_3 episodes in the PRD can be typically divided into two periods, as stagnation leads to the accumulation of locally produced O_3 in the first phase and strong northerly winds strengthen O_3 transport before the landing of typhoons (Lam et al., 2005; Li, 2013). It should be noted that updrafts, rather than downdrafts, prevailed on the typhoon-induced O_3 pollution days in summer. High levels of O_3 did not necessarily occur in the regions dominated by downdrafts in this scenario, suggesting a less notable connection between downdrafts and summertime O_3 pollution in the PRD. Further investigations are required to trace the detailed process of downward O_3 transport, including the stratosphere-troposphere exchange (Stohl et al., 2003), in each scenario, and quantify their contributions to near-ground O_3 pollution.

Some limitations remain in this study. We chose O_3 pollution days as individual samples, ignoring the influence of O_3 pollution on the previous days. Thus, more detailed full-episode analyses are required. Moreover, owing to the small sampling size, the influence of typhoons on O_3 pollution in the PRD is still not fully understood, including, for instance, the detailed connections between the features of typhoons (intensity, position) and O_3 pollution. However, the comparisons of meteorological conditions, O_3 processes and sources in different scenarios and seasons demonstrate the complex causes of typhoon-induced O_3 pollution in the PRD — typhoons tend to enhance O_3 transport into the PRD in both seasons, but their impacts on the production and accumulation of O_3 are completely different. As a result, emissions within (outside of) the PRD are likely to contribute less (more) on the typhoon-induced O_3 pollution days than on the no-typhoon days. In order to effectively alleviate O_3 pollution and to reduce the population exposure in the PRD, more attention should be paid to controlling anthropogenic emissions of O_3 precursors on a larger scale, rather than focusing on local emission, under typhoon influence. For air quality management, it is suggested to comprehensively evaluate the response of O_3 levels in the PRD to fractional local and non-local emission reductions so as to find the most effective strategies to alleviate O_3 pollution in different scenarios (Thunis et al., 2019; Thunis et al., 2020). This study also suggests that a thorough evaluation of O_3 transport, production and accumulation conditions can be applied to understand the causes of regional O_3 pollution not only in the PRD, but also in other regions. The results will help find efficient strategies to alleviate regional O_3 pollution as well as to reduce its adverse effects.

Data availability. Data are available from the corresponding author upon request.

Author contributions. KQ, XW and YZ designed the study. KQ, XW, and TX did the simulation work, including the operation of the WRF, SMOKE and CMAQ models. JS, HD, LZ and YZ provided observational results of field campaigns and the routine monitoring datasets for the evaluation of model performance. KQ, XW, YY and YZ analysed the modelling results. KQ, XW, YY and YZ wrote and revised this paper, with critical feedbacks from all other authors.

Competing interests. The authors declare no conflict of interest.

Acknowledgements. This work was supported by the National Key Research and Development Program of China (Grant No. 2018YFC0213204, 2018YFC0213506, 2018YFC0213501) and the National Science and Technology Pillar Program of China (Grant No. 2014BAC21B01).

References

Berrisford, P., Dee, D., Poli, P., Brugge, R., Fielding, K., Fuentes, M., Kallberg, P., Kobayashi, S., Uppala, S., and Simmons, A.: The ERA-Interim archive Version 2.0, ERA report series, 1, 1–16, 2011.

Carter, W. P. L.: Development of the SAPRC-07 chemical mechanism, Atmos. Environ., 44, 5324–5335, https://doi.org/10.1016/j.atmosenv.2010.01.026, 2010.

Chen, H., Wang, X., Shen, J., Lu, K., and Zhang, Y.: Ozone source apportionment of typical photochemical pollution episodes in the Pearl River Delta in autumn, Acta Scientiarum Naturalium Universitatis Pekinensis (in Chinese), 51, 620–630, https://doi.org/10.13209/j.0479-8023.2015.089, 2015.

Chen, Q., Miao, J., and Li, W.: A comparison of mean wind field and mean meridional circulation between south-west monsoon area in Southeast Asia and Pacific trade wind area in July, 1958, Acta Meteorologica Sinica (in Chinese), 34(1), 51–61, https://doi.org/10.11676/qxxb1964.006, 1964.

Chen, X., Liu, Y., Lai, A., Han, S., Fan, Q., Wang, X., Ling, Z., Huang, F., and Fan, S.: Factors dominating 3-dimensional ozone distribution during high tropospheric ozone period, Environ. Pollut., 232, 55–64, https://doi.org/10.1016/j.envpol.2017.09.017, 2018.

Chow, E. C., Li, R. C., and Zhou, W.: Influence of tropical cyclones on Hong Kong air quality, Adv. Atmos. Sci., 35(9), 1177–1188, https://doi.org/10.1007/s00376-018-7225-4, 2018.

Chow, E. C., Wen, M., Li, L., Leung, M. Y., Cheung, P. K., and Zhou, W.: Assessment of the Environmental and Societal Impacts of the Category-3 Typhoon Hato, Atmosphere, 10(6), 296. https://doi.org/10.3390/atmos10060296, 2019.

Clappier, A., Belis, C. A., Pernigotti, D., and Thunis, P.: Source apportionment and sensitivity analysis: two methodologies with two different purposes, Geosci. Model Dev., 10, 4245–4256, https://doi.org/10.5194/gmd-10-4245-2017, 2017.

Dee, D. P., Uppala, S. M., Simmons, A. J., Berrisford, P., Poli, P., Kobayashi, S., Andrae, U., Balmaseda, M. A., Balsamo, G., Bauer, P., Bechtold, P., Beijaars, A.C.M., van de Berg, L., Bidiot, J., Bormann, N., Delsol, C., Dragani, R., Fuentes, M., Geer, A.J., Haimberger, L., Healy, S.B., Hersbach, H., Hólm, E.V., Isaksen, L., Isaksen, L., Kållberg, P., Köhler, M., Matricardi, M., McNally, A.P., Monge-Sanz, B.M., Morcrette, J.-J., Park, B.-K., Peubey, C., de Rosnay, P., Tavolato, Thépaut, J.-N., and Vitart, F.: The ERA−Interim reanalysis: Configuration and performance of the data assimilation system, Q. J. Roy. Meteor. Soc., 137(656), 553–597, https://doi.org/10.1002/qj.828, 2011.

Deng, T., Wang, T., Wang, S., Zou, Y., Yin, C., Li, F., Liu, L., Wang, N., Song, L., Wu, C., and Wu, D.: Impact of typhoon periphery on high ozone and high aerosol pollution in the Pearl River Delta region, Sci. Total Environ., 668, 617–630, https://doi.org/10.1016/j.scitotenv.2019.02.450, 2019.

Ding, Y. H.: Monsoons over China, Kluwer Academic Publishers, Dordrecht/Boston/London, 1994.

Ding, Y., Si, D., Liu, Y., Wang, Z., Li, Y., Zhao, L., and Song, Y.: On the Characteristics, Driving Forces and Inter-decadal Variability of the East Asian Summer Monsoon, Chinese Journal of Atmospheric Sciences (in Chinese), 42(3), 533–558, https://doi.org/10.3878/j.issn.1006-9895.1712.17261, 2018.

Feng, Y., Ning, M., Lei, Y., Sun, Y., Liu, W., and Wang, J.: Defending blue sky in China: Effectiveness of the "Air Pollution Prevention and Control Action Plan" on air quality improvements from 2013 to 2017, J. Environ. Manage., 252, 109603, https://doi.org/10.1016/j.jenvman.2019.109603, 2019.

Gao, X., Deng, X., Tan, H., Wang, C., Wang, N., and Yue, D.: Characteristics and analysis on regional pollution process and circulation weather types over Guangdong Province, Acta Scientiae Circumstantiae (in Chinese), 38(5), 1708–1716, https://doi.org/10.13671/j.hjkxxb.2017.0473, 2018.

Guo, J., Miao, Y., Zhang, Y., Liu, H., Li, Z., Zhang, W., He, J., Lou, M., Yan, Y., Bian, L., and Zhai, P.: The climatology of planetary boundary layer height in China derived from radiosonde and reanalysis data, Atmos. Chem. Phys., 16, 13309–13319, https://doi.org/10.5194/acp-16-13309-2016, 2016.

He, K.: Multi-resolution Emission Inventory for China (MEIC): model framework and 1990-2010 anthropogenic emissions, American Geophysical Union, Fall Meeting 2012, San Francisco, the United States of America, 3–7 December 2012, A32B-05, 2012.

He Y. J., Uno, I., Wang, Z. F., Pochanart, P., Li, J., and Akimoto, H.: Significant impact of the East Asia monsoon on ozone seasonal behavior in the boundary layer of Eastern China and the west Pacific region, Atmos. Chem. Phys., 8, 7543–7555, https://doi.org/10.5194/acp-8-7543-2008, 2008.

Huang, J. P., Fung, J. C., Lau, A. K., and Qin, Y: Numerical simulation and process analysis of typhoon‐related ozone episodes in Hong Kong, J. Geophys. Res.-Atmos., 110(D5), https://doi.org/10.1029/2004JD004914, 2005.

Huang, Y., Yao, T., Fung, J. C., Lu, X., and Lau, A. K.: Application of air parcel residence time analysis for air pollution prevention and control policy in the Pearl River Delta region, Sci. Total Environ., 658, 744–752, https://doi.org/10.1016/j.scitotenv.2018.12.205, 2019.

Jin, Q., Yang, X. Q., Sun, X. G., and Fang, J. B.: East Asian summer monsoon circulation structure controlled by feedback of condensational heating, Clim. Dynam., 41(7-8), 1885–1897, https://doi.org/10.1007/s00382-012-1620-9, 2013.

Jiang, F., Wang, T., Wang, T., Xie, M., and Zhao, H.: Numerical modeling of a continuous photochemical pollution episode in Hong Kong using WRF–chem, Atmos. Environ., 42(38), 8717–8727, https://doi.org/10.1016/j.atmosenv.2008.08.034, 2008.

Lam, K. S., Wang, T. J., Wu, C. L., and Li, Y. S.: Study on an ozone episode in hot season in Hong Kong and transboundary air pollution over Pearl River Delta region of China, Atmos. Environ., 39(11), 1967–1977, https://doi.org/10.1016/j.atmosenv.2004.11.023, 2005.

Lam, Y. F.: Climate change and air quality in Southeastern China: Hong Kong study, in: Climate change and air pollution, edited by: Akhtar R., and Palagiano C., Springer, Cham, 181–196, https://doi.org/10.1007/978-3-319-61346-8_12, 2018.

Lam, Y. F., Cheung, H. M., and Ying, C. C.: Impact of tropical cyclone track change on regional air quality, Sci. Total Environ., 610, 1347–1355, https://doi.org/10.1016/j.scitotenv.2017.08.100, 2018.

584 Li, J., Lu, K., Lv, W., Li, J., Zhong, L., Ou, Y., Chen, D., Huang, X., and Zhang, Y.: Fast increasing of surface ozone
585 concentrations in Pearl River Delta characterized by a regional air quality monitoring network during 2006–2011, J.
586 Environ. Sci., 26(1), 23–36, https://doi.org/10.1016/S1001-0742(13)60377-0, 2014.
587 Li, M., Jiang, S., Gan, Q., Chen, F., Zeng, D., Li, J., Fan, S., and Zhu, W.: Characteristics of ozone pollution and analysis of
588 typical pollution processes in summer and autumn in Huizhou, Acta Scientiarum Naturalium Universitatis Sunyatseni
589 (in Chinese), 57(5), 29, https://doi.org/10.13471/j.cnki.acta.snus.2018.05.004, 2018.
590 Li, M., Zhang, Q., Kurokawa, J.-I., Woo, J.-H., He, K., Lu, Z., Ohara, T., Song, Y., Streets, D. G., Carmichael, G. R., Cheng,
591 Y., Hong, C., Huo, H., Jiang, X., Kang, S., Liu, F., Su, H., and Zheng, B.: MIX: a mosaic Asian anthropogenic emission
592 inventory under the international collaboration framework of the MICS-Asia and HTAP, Atmos. Chem. Phys., 17, 935–
593 963, https://doi.org/10.5194/acp-17-935-2017, 2017.
594 Li, K., Jacob, D. J., Liao, H., Shen, L., Zhang, Q., and Bates, K. H.: Anthropogenic drivers of 2013–2017 trends in summer
595 surface ozone in China, P. Natl. Acad. Sci. USA, 116(2), 422–427, https://doi.org/10.1073/pnas.1812168116, 2019.
596 Li, Y.: The evolution characteristics and source analysis of the secondary pollutants in summer over Pearl River Delta, Ph.D.
597 thesis, College of Environmental Science and Engineering, Peking University, China, 160 pp., 2013.
598 Li, Y., Lau, A. K. H., Fung, J. C. H., Zheng, J.Y., Zhong, L. J., and Louie, P. K. K.: Ozone source apportionment (OSAT) to
599 differentiate local regional and super-regional source contributions in the Pearl River Delta region, China, J. Geophys.
600 Res.-Atmos., 117, D15305, http://doi.org/10.1029/2011JD017340, 2012.
601 Liou, K. N.: On the absorption, reflection and transmission of solar radiation in cloudy atmospheres, J. Atmos. Sci., 33(5),
602 798–805, https://doi.org/10.1175/1520-0469(1976)033<0798:OTARAT>2.0.CO;2, 1976.
603 Lin, X., Yuan, Z., Yang, L., Luo, H., and Li, W.: Impact of extreme meteorological events on ozone in the Pearl River Delta,
604 China, Aerosol Air Qual. Res., 19(6), 1307–1324, https://doi.org/10.4209/aaqr.2019.01.0027, 2019.
605 Liu, H., Liu, S., Xue, B., Lv, Z., Meng, Z., Yang, X., Xue, T., Yu, Q., and He, K.: Ground-level ozone pollution and its
606 health impacts in China, Atmos. Environ., 173, 223–230, https://doi.org/10.1016/j.atmosenv.2017.11.014, 2018.
607 Lu, X., Hong, J., Zhang, L., Cooper, O. R., Schultz, M. G., Xu, X., Wang, T., Gao, M., Zhao, Y., and Zhang, Y.: Severe
608 surface ozone pollution in China: A global perspective, Environ. Sci. Tech. Let., 5(8), 487–494,
609 https://doi.org/10.1021/acs.estlett.8b00366, 2018.
610 Mills, G., Sharps, K., Simpson, D., Pleijel, H., Broberg, M., Uddling, J., Jaramillo, F., Davies, W. J., Dentener, F., Van den
611 Berg, M., Agrawal, M., Agrawal, S. B., Ainsworth, E. A., Büker, P., Emberson, L., Feng, Z., Harmens, H., Hayes, F.,
612 Kobayashi, K., Paoletti, E., and Van Dingenen, R.: Ozone pollution will compromise efforts to increase global wheat
613 production, Glob. Change Biol., 24, 3560–3574, https://doi.org/10.1111/gcb.14157, 2018.
614 National Research Council: Rethinking the Ozone Problem in Urban and Regional Air Pollution, Natl. Acad. Press,
615 Washington, D. C., USA, 1991.

Park, S. K., O'Neill, M. S., Stunder, B. J., Vokonas, P. S., Sparrow, D., Koutrakis, P., and Schwartz, J.: Source location of air pollution and cardiac autonomic function: trajectory cluster analysis for exposure assessment, J. Expo. Sci. Env. Epid., 17(5), 488-497, https://doi.org/10.1038/sj.jes.7500552, 2007.

Roux, F., Clark, H., Wang, K.-Y., Rohs, S., Sauvage, B., and Nédélec, P.: The influence of typhoons on atmospheric composition deduced from IAGOS measurements over Taipei, Atmos. Chem. Phys., 20, 3945–3963, https://doi.org/10.5194/acp-20-3945-2020, 2020.

So, K. L. and Wang, T.: On the local and regional influence on ground-level ozone concentrations in Hong Kong, Environ. Pollut., 123(2), 307–317, https://doi.org/10.1016/S0269-7491(02)00370-6, 2003.

Stein, A. F., Draxler, R. R., Rolph, G. D., Stunder, B. J., Cohen, M. D., and Ngan, F.: NOAA's HYSPLIT atmospheric transport and dispersion modeling system, B. Am. Meteorol. Soc., 96(12), 2059–2077, https://doi.org/10.1175/BAMS-D-14-00110.1, 2015.

Stevenson, D. S., Dentener, F. J., Schultz, M. G., Ellingsen, K., van Noije, T. P. C., Wild, O., Zeng, G., Amann, M., therton, C. S., Bell, N., Bergmann, D. J., Bey, I., Butler, T., Cofala, J., Collins, W. J., Derwent, R. G., Doherty, R. M., Drevet, J., Eskes, H. J., Fiore, A. M., Gauss, M., Hauglustaine, D. A., Horowitz, L. W., Isaksen, I. S. A., Krol, M. C., Lamarque, J.-F., Lawrence, M. G., Montanaro, V., Müller, J.-F., Pitari, G., Prather, M. J., Pyle, J. A., Rast, S., Rodriguez, J. M., Sanderson, M. G., Savage, N. H., Shindell, D. T., Strahan, S. E., Sudo, K., and Szopa, S.: Multimodel ensemble simulations of present-day and near-future tropospheric ozone, J. Geophys. Res., 111, D08301, https://doi.org/10.1029/2005JD006338, 2006.

Stohl, A., Bonasoni, P., Cristofanelli, P., Collins, W., Feichter, J., Frank, A., Forster, C., Gerasopoulos, E., Gaggeler, H., James, P., Kentarchos, T., Kromp-Kolb, H., Kruger, B., Land, C., Meloen, J., Papayannis, A., Priller, A., Seibert, P., Sprenger, M., Roelofs, G. J., Scheel, H. E., Schnabel, C., Siegmund, P., Tobler, L., Trickl, T., Wernli, H., Wirth, V., Zanis, P., and Zerefos, C.: Stratosphere-troposphere exchange: A review, and what we have learned from STACCATO, J. Geophys. Res., 108, 8516, https://doi.org/10.1029/2002JD002490, 2003.

Thunis, P., Clappier, A., Pirovano, G.: Source apportionment to support air quality management practices, A fitness-for-purpose guide (V 3.1), EUR30263, Publications Office of the European Union, ISBN 978-92-76-19744-7, doi:10.2760/47145, JRC120764, 2020.

Thunis, P., Clappier, A., Tarrason, L., Cuvelier, C., Monteiro, A., Pisoni, E., Wesseling, J., Belis, C. A., Pirovano, G., Janssen, S., Guerreiro, C., and Peduzzi, E.: Source apportionment to support air quality planning: Strengths and weaknesses of existing approaches, Environ. Int., 130, 104825, https://doi.org/10.1016/j.envint.2019.05.019, 2019.

Wang, H., Wang, W., Huang, X., and Ding A.: Impacts of stratosphere-to-troposphere-transport on summertime surface ozone over eastern China, Sci. Bull., 65, 276–279, https://doi.org/10.1016/j.scib.2019.11.017, 2020.

Wang, N., Guo, H., Jiang, F., Ling, Z. H., and Wang, T.: Simulation of ozone formation at different elevations in mountainous area of Hong Kong using WRF-CMAQ model, Sci. Total Environ., 505, 939–951, https://doi.org/10.1016/j.scitotenv.2014.10.070, 2015.

650 Wang, T. and Kwok, J. Y: Measurement and analysis of a multiday photochemical smog episode in the Pearl River Delta of
651 China, J. Appl. Meteorol., 42(3), 404–416, https://doi.org/10.1175/1520-0450(2003)042<0404:MAAOAM>2.0.CO;2,
652 2003.
653 Wang, T., Lam, K. S., Lee, A. S., Pang, S. W., and Tsui, W. S.: Meteorological and chemical characteristics of the
654 photochemical ozone episodes observed at Cape D'Aguilar in Hong Kong, J. Appl. Meteorol., 37(10), 1167–1178,
655 https://doi.org/10.1175/1520-0450(1998)037<1167:MACCOT>2.0.CO;2, 1998.
656 Wang, T., Wu, Y. Y., Cheung, T. F., and Lam, K. S.: A study of surface ozone and the relation to complex wind flow in
657 Hong Kong, Atmos. Environ., 35(18), 3203–3215, https://doi.org/10.1016/S1352-2310(00)00558-6, 2001.
658 Wang, T., Xue, L., Brimblecombe, P., Lam, Y. F., Li, L., and Zhang, L.: Ozone pollution in China: A review of
659 concentrations, meteorological influences, chemical precursors, and effects, Sci. Total Environ., 575, 1582–1596,
660 https://doi.org/10.1016/j.scitotenv.2016.10.081, 2017.
661 Wang, X., Zhang, Y., Hu, Y., Zhou, W., Lu, K., Zhong, L., Zeng, L., Shao, M., Hu, M., and Russell, A. G.: Process analysis
662 and sensitivity study of regional ozone formation over the Pearl River Delta, China, during the PRIDE-PRD2004
663 campaign using the Community Multiscale Air Quality modeling system, Atmos. Chem. Phys., 10, 4423–4437,
664 https://doi.org/10.5194/acp-10-4423-2010, 2010.
665 Wei, X., Lam, K. S., Cao, C., Li, H., and He, J.: Dynamics of the typhoon Haitang related high ozone episode over Hong
666 Kong, Adv. Meteorol., 2016, https://doi.org/10.1155/2016/6089154, 2016.
667 Yang, J. X., Lau, A. K. H., Fung, J. C. H., Zhou, W., and Wenig, M.: An air pollution episode and its formation mechanism
668 during the tropical cyclone Nuri's landfall in a coastal city of south China, Atmos. Environ., 54, 746–753,
669 https://doi.org/10.1016/j.atmosenv.2011.12.023, 2012.
670 Ying, M., Zhang, W., Yu, H., Lu, X., Feng, J., Fan, Y., Zhu, Y., and Chen, D.: An overview of the China Meteorological
671 Administration tropical cyclone database, J. Atmos. Ocean Tech., 31(2), 287–301, https://doi.org/10.1175/JTECH-D-
672 12-00119.1, 2014.
673 Yue, H., Gu, T., Wang, C., Wu, D., Deng, X., Huang, J., and Wang, Y.: Influence of typhoon Nida process on ozone
674 concentration in Guangzhou, Acta Scientiae Circumstantiae (in Chinese), 38(12), 4565–4572,
675 https://doi.org/10.13671/j.hjkxxb.2018.0319, 2018.
676 Zhang, X., Liu, Y., Deng, X., Chen, P., Feng, Y., and Fan, Q.: Analysis of summertime typical pollution in Pearl River Delta
677 region——numerical simulation of meteorological field, Meteorological and Environmental Research, 59(4), 9–18,
678 2014.
679 Zhao, W., Gao, B., Liu, M., Lu, Q., Ma, S., Sun, S., Sun, J. Chen, L., and Fan, S.: Impact of meteorological factors on the
680 ozone pollution in Hong Kong, Huan jing ke xue= Huanjing kexue (in Chinese), 40(1), 55–66,
681 https://doi.org/10.13227/j.hjkx.201803151, 2019.

682 Zheng, J., Zhang, L., Che, W., Zheng, Z., and Yin, S.: A highly resolved temporal and spatial air pollutant emission
683 inventory for the Pearl River Delta region, China and its uncertainty assessment, Atmos. Environ., 43(32), 5112–5122,
684 https://doi.org/10.1016/j.atmosenv.2009.04.060, 2009.
685 Zheng, J., Zhong, L., Wang, T., Louie, P. K. K., and Li, Z.: Ground-level ozone in the Pearl River Delta region: Analysis of
686 data from a recently estabilished regional air quality monitoring network, Atmos. Environ., 44(6), 814–823,
687 https://doi.org/10.1016/j.atmosenv.2009.11.032, 2010.